

Bubble Detection with Application to Green Bubbles: a Noncausal Approach

Francesco Giancaterini^{*}, Alain Hecq[†], Joann Jasiak[‡], Aryan Manafi Neyazi[§]

June 9, 2025

Abstract

This paper introduces a new approach to detect bubbles based on mixed causal and noncausal processes and their tail process representation during explosive episodes. Departing from traditional definitions of bubbles as nonstationary and temporarily explosive processes, we adopt a perspective in which prices are viewed as following a strictly stationary process, with the bubble considered an intrinsic component of its non-linear dynamics. We illustrate our approach on the phenomenon referred to as the "green bubble" in the field of renewable energy investment.

Keywords: Green bubbles, Noncausal models, Non-Gaussianity, GCov estimator

JEL: C22

^{*}Centre for Economic and International Studies, Tor Vergata University of Rome, Italy, email: francesco.giancaterini@uniroma2.it

[†]Department of Quantitative Economics, Maastricht University, The Netherlands, email: a.hecq@maastrichtuniversity.nl

[‡]Department of Economics, York University, Canada, e-mail: jasiakj@yorku.ca

[§]Department of Economics, York University, Canada, e-mail: aryanmn@yorku.ca

The authors acknowledge financial support of Natural Sciences and Engineering Council (NSERC) and MITACS of Canada and thank C. Gouriéroux for helpful comments.

1 Introduction

This paper introduces a novel method of bubble detection based on strictly stationary non-causal processes and their tail process representation during a bubble. The tail process was first defined by [Basrak and Segers \(2009\)](#) as the weak limit of finite-dimensional distributions of the time series, given that an extreme value occurs at time 0. This definition was further generalized to the tail empirical process by [Kulik and Soulier \(2020\)](#), which is based solely on observations exceeding a high threshold. It is valid for geometrically ergodic Markov processes, and consequently also for mixed causal-noncausal autoregressive $MAR(1,1)$ and purely noncausal $MAR(0,1)$ processes – where the notation $MAR(r, s)$ indicates a mixed model with r indicating the causal order and s the noncausal one – with locally explosive patterns including bubbles and spikes. As shown for example, by [Fries and Zakoian \(2019\)](#) and [Cavaliere et al. \(2020\)](#), $MAR(1,1)$ and $MAR(0,1)$ processes are well-suited for modeling variables such as commodity and cryptocurrency prices. In this context, the paper introduces a simple statistic that provides an ex-ante warning of a potentially emerging bubble. Ex-post, this statistic is a tool to measure the bubble’s duration and identify its starting and ending dates.

Alternative methods for detecting bubbles include Augmented Dickey-Fuller-type tests (e.g., SADF and GSADF), which assess unit roots and explosive regimes [[Phillips et al. \(2011\)](#); [Phillips et al. \(2015\)](#)]. However, our approach departs from these conventional methods by employing mixed autoregressive causal-noncausal models, which capture locally explosive patterns observed in the data. Unlike those detection approaches, we assume that the series follows a strictly stationary process in which bubbles are an inherent part of the dynamics.

The rest of the paper is organized as follows. Section 2 reviews the causal-noncausal autoregressive processes and their estimation techniques, with a focus on the GCov estimator. Section 3 studies the behavior of the MAR process and its tail dynamics when series are in a bubble period. Section 4 develops test statistics to detect significant bubbles and to isolate them from short spikes. In Section 5, we apply our innovative strategy to investigate the presence and duration of ”green bubbles” in the green energy stock market. Section 6 concludes.

2 Causal-Noncausal Processes

The causal-noncausal models represent stationary processes characterized by locally explosive patterns in their paths, such as bubbles and spikes. The univariate causal-noncausal

models were examined e.g. by [Breidt et al. \(1991\)](#) and [Lanne and Saikkonen \(2011\)](#), and extended to multivariate analysis by [Lanne and Saikkonen \(2013\)](#), [Gourieroux and Jasiak \(2017\)](#), and [Davis and Song \(2020\)](#). In applied research the causal-noncausal models were used to study various economic and financial variables, including Bitcoin prices [[Hencic and Gouriéroux \(2015\)](#), [Cavaliere et al. \(2020\)](#)], stock market indices [[Gourieroux and Zakoian \(2017\)](#)], commodity prices [[Hecq and Voisin \(2021\)](#), [Lof and Nyberg \(2017\)](#)], and inflation rates [[Lanne and Saikkonen \(2013\)](#), [Hecq and Voisin \(2023\)](#)].

The advantage of causal-noncausal models is that they capture complex nonlinear patterns, including local trends and conditional heteroskedasticity, even though their specification resembles traditional linear time series. However, the traditional Box-Jenkins approach for identifying and estimating linear time series processes does not apply to this class of models because it is valid under the assumption of Gaussian errors, while under the Gaussianity assumption, the causal and noncausal dynamics cannot be distinguished; see [Gourieroux and Monfort \(2015\)](#). Hence, for the identification, we assume non-Gaussian error distributions in the causal-noncausal processes.

2.1 Univariate Causal-Noncausal Models

A strictly univariate mixed causal-noncausal autoregressive $MAR(r, s)$ model is defined as:

$$\Phi(L)\Psi(L^{-1})y_t = \epsilon_t, \quad (1)$$

where the error terms ϵ_t are non-Gaussian, independent, identically distributed (i.i.d.) and such that $E(|\epsilon_t|^\delta) < 1$ for $\delta > 0$ [[Lanne and Saikkonen \(2011\)](#)]. The polynomial $\Phi(L)$ in the lag operator L is of order r . The polynomial $\Psi(L^{-1})$ in the lead operator L^{-1} is of order s . Both polynomials $\Phi(L)$ and $\Psi(L^{-1})$ have their roots outside the unit circle.

The $MAR(r, s)$ process (1) admits a unique strictly stationary solution, which is a two-sided moving average of order infinity $MA(\infty)$:

$$y_t = \sum_{h=-\infty}^{\infty} c_h \epsilon_{t+h},$$

In the past, present, and future shocks, with $c_0 = 1$ [[Breidt et al. \(1991\)](#)]. The coefficients c_h are uniquely defined provided that (ϵ_t) are non-Gaussian. When y_t is purely causal (resp. noncausal), the coefficients c_h are zero for all $h > 0$ (resp. $h < 0$). Thus, a purely causal process is determined only by the past and present shocks, while a purely noncausal process is influenced only by the present and future shocks. For $r = s = 1$, we obtain the $MAR(1, 1)$ process:

$$(1 - \phi L)(1 - \psi L^{-1})y_t = \epsilon_t, \quad (2)$$

with $|\psi| < 1, |\phi| < 1$, which is purely causal (resp. noncausal) if $\psi = 0$ (resp. $\phi = 0$). For each of these pure process, the effects of a large ϵ_t are easily distinguished, as a large error leads to a (vertical) jump if $\psi = 0$ and $\phi > 0$, and an explosive bubble with a (vertical) burst if $\psi > 0$ and $\phi = 0$. In the mixed MAR(1,1), a bubble grows at the rate $1/\psi^h$ and bursts at the rate ϕ^h .

The MAR(1,1) process can be decomposed into the following unobserved components [Lanne and Saikkonen (2011)]:

$$u_t \equiv (1 - \phi L)y_t \text{ or, } (1 - \psi L^{-1})u_t = \epsilon_t, \quad (3)$$

and

$$v_t \equiv (1 - \psi L^{-1})y_t \text{ or, } (1 - \phi L)v_t = \epsilon_t. \quad (4)$$

Gourieroux and Jasiak (2016) shows that u_t is ϵ -noncausal (dependent on the future and present values of ϵ) and y -causal (dependent on the past and present values of y), representing the explosive part of the process, including bubbles and spikes. In contrast, v_t is ϵ -causal (dependent on the past and present values of ϵ) and y -noncausal (dependent on the future and present values of y), representing the regular dynamics of y_t . Thus, u_t, v_t are the causal and noncausal components of y_t .

The process y_t can be described by the following deterministic representation based on the unobserved components:

$$y_t = \frac{1}{1 - \phi\psi}(\phi v_{t-1} + u_t), \text{ or } y_t = \frac{1}{1 - \phi\psi}(v_t + \psi u_{t+1}).$$

We observe that y_t is a linear function of the first lag of the ϵ -causal component v_t and of the current value of the ϵ -noncausal component u_t . Alternatively, y_t can be expressed as a linear function of the current value of the ϵ -causal component v_t and of the first lag of the ϵ -noncausal component u_t . The noncausal component v_t represents the explosive part of the process, such as bubbles and spikes. On the other hand, u_t is the purely causal component of process y_t .

Remark 1: An alternative univariate representation of the causal-noncausal process can be written as:

$$y_t = \varphi_1 y_{t-1} - \cdots - \varphi_p y_{t-p} + \varepsilon_t,$$

where $\varepsilon_t = -\frac{1}{\psi_s}\epsilon_t$ [Brockwell and Davis (1997)]. In this model, the polynomial $\Phi(L) = 1 - \varphi_1 L - \dots - \varphi_p L^p$ has roots both inside and outside the unit circle. Specifically, the roots outside the unit circle correspond to the causal component of y_t , while the roots inside the unit circle indicate the noncausal component capturing the bubbles and other nonlinear features. Note that in either representation of the model, the error ε_t is not an innovation process because ε_t is not independent of y_{t-1}, y_{t-2}, \dots . This representation is the cornerstone of the GCov estimator presented in the next subsection.

2.2 The GCov Estimator

One way to estimate and identify $\text{MAR}(r, s)$ models is by using a parametric non-Gaussian MLE approach (see e.g. [Hecq et al. \(2016\)](#)). Instead, the Generalized Covariance (GCov) estimator is a semi-parametric estimator that does not require any distributional assumptions on the errors, other than the non-Gaussianity for the identification of parameters. It is a one-step estimator that is consistent, asymptotically normally distributed, and semi-parametrically efficient. It can achieve parametric efficiency in special cases [[Gourieroux and Jasiak \(2023\)](#)]. The GCov minimizes a portmanteau-type objective function involving nonlinear autocovariances, i.e., the autocovariances of nonlinear transformations of model errors, which successfully identify the causal and noncausal dynamics [[Chan et al. \(2006\)](#)].

For instance, we consider nonlinear functions $a(\varepsilon_t) = [a_1(\varepsilon_t)', \dots, a_K(\varepsilon_t)']$ that satisfy the regularity conditions given in [Gourieroux and Jasiak \(2023\)](#). This increases the dimension of the process from 1 to K . Let us denote by $\hat{\Gamma}^a(h; \theta), h = 1, \dots, H$ the autocovariance matrices at lags $h = 0, \dots, H$, with $\hat{\Gamma}^a(0; \theta)$ representing the variance. Then, the GCov estimator of the parameter θ_T minimizes the following objective function:

$$\hat{\theta}_T = \underset{\theta}{\operatorname{argmin}} \sum_{h=1}^H \operatorname{Tr} \left[\hat{\Gamma}^a(h; \theta) \hat{\Gamma}^a(0; \theta)^{-1} \hat{\Gamma}^a(h; \theta)' \hat{\Gamma}^a(0; \theta)^{-1} \right], \quad (5)$$

where Tr denotes the trace of a matrix and we denote $L_T(\hat{\theta}_T, H)$ the value of the function at its minimum. Alternatively when the number of transformations K is large, we can replace in the above formula $\hat{\Gamma}^a(0; \theta)$ with $\operatorname{diag}(\hat{\Gamma}_d(0; \theta))$, which is the variance matrix containing solely the diagonal elements of $\hat{\Gamma}_a(0; \theta)$. This latter version of the GCov estimator is no longer semi-parametrically efficient, as it is not optimally weighted [see [Gourieroux and Jasiak \(2023\)](#), [Cubadda and Hecq \(2011\)](#)]. Another strategy for the diagonal GCov is the regularized GCov proposed by [Giancaterini et al. \(2025\)](#).

The choice of an informative set of transformations $(a_k, k = 1, \dots, K)$ depends on the specific series under investigation. For example, in financial applications that aim to capture

the absence of a leverage effect, one can select both linear and quadratic functions. For a bivariate process with $n = 2$, we may consider the following set of four functions ($J = 4$): $a_1(\varepsilon_t) = \varepsilon_{1,t}$, $a_2(\varepsilon_t) = \varepsilon_{2,t}$, $a_3(\varepsilon_t) = \varepsilon_{1,t}^2$ and $a_4(\varepsilon_t) = \varepsilon_{2,t}^2$. This implies that a_1 and a_2 are linear functions of errors in a causal-noncausal process, while a_3 transforms the error term by squaring it for each $t = 1, \dots, T$, where T represents the total number of observations.

Moreover, the objective function minimized in (5) and evaluated at the estimated parameter $\hat{\boldsymbol{\theta}}_T$ can be used for testing the fit of the model. Specifically, we test the null hypothesis:

$$H_0 : \{\Gamma_0^a(h) = 0, h = 1, \dots, H\},$$

using the statistic

$$\hat{\xi}_T(H) = TL_T(\hat{\boldsymbol{\theta}}_T, H),$$

which under the implicit null hypothesis of serial independence of errors has an asymptotic chi-square distribution with the degrees of freedom equal to $HK^2 - \dim(\boldsymbol{\theta})$ [Gourieroux and Jasiak (2023)].

3 Bubble Analysis

Our approach to bubble analysis assumes that the process follows a strictly stationary $\text{MAR}(r, s)$ process with errors from a heavy-tailed distribution with tail parameter $\alpha \in (0, 2)$ that includes the Cauchy distribution for $\alpha = 1$, for example. In this Section, we focus our attention on MAR processes of orders r and s less than or equal to 1, so that the process of interest is either a $\text{MAR}(0,1)$, i.e., a purely noncausal process of order 1, or a $\text{MAR}(1,1)$. These processes are geometrically ergodic. [Gourieroux and Zakoian \(2017\)](#) and [Fries and Zakoian \(2019\)](#) also show that the $\text{MAR}(0,1)$ and $\text{MAR}(1,1)$ processes are Markov of order 1 and 2, respectively. The results can be generalized to higher-order $\text{MAR}(r, s)$ processes, which are Markov too [[Fries and Zakoian \(2019\)](#), Proposition 3.1].

3.1 On-Bubble Dynamics

Let us consider the locally explosive $\text{MAR}(0,1)$ and $\text{MAR}(1,1)$ processes. It has been shown in the literature that during a bubble episode, and conditional on a large $y_t > y$, the causal-noncausal $\text{MAR}(0,1)$ and $\text{MAR}(1,1)$ processes with α -stable distributed errors, $\alpha \in (0, 2)$ have distinct dynamics [[Fries \(2022\)](#)]. Let us describe these dynamics and generalize the results in [Fries \(2022\)](#) using the concept of a spectral tail process, based only on observations above a high threshold. We have the following result:

Proposition 1 [Kulik and Soulier (2020), Chapter 15.3]: Let $\{y_t, t \in \mathbb{Z}\}$ be a strictly stationary process with i.i.d. errors $\epsilon_t, t = 1, 2, \dots$ from a heavy-tailed distribution with Pareto-type tails of tail index α and with a two-sided MA representation:

$$y_t = \sum_{h=-\infty}^{+\infty} c_h \epsilon_{t-h},$$

with nonnegative coefficients. The process $\left(\frac{y_{t+h}}{y_t}\right)_h, h \in \mathbb{Z}$, converges weakly to the (spectral) tail process (X_h) , so that conditional on a large $y_t > y$, where y is a high threshold, we have :

$$\mathcal{L}\left(\frac{y_{t+h}}{y_t}, h = -H, \dots, H | y_t > y\right) \xrightarrow{w} \mathcal{L}(X_h, h = -H, \dots, H),$$

where \xrightarrow{w} denotes weak convergence, also denoted as $\frac{y_{t+h}}{y_t} \xrightarrow{d} X_h$ for $h \in \mathbb{Z}$, and

$$X_h = \frac{c_{h+N}}{c_N} X_0, \quad h \in \mathbb{Z}, \quad (6)$$

where $X_0 = 1$ and N is an integer-valued random variable, independent of y and such that:

$$P[N = h] = \frac{c_h^\alpha}{\sum_{h \in \mathbb{Z}} c_h^\alpha}, \quad \forall h \in \mathbb{Z}. \quad (7)$$

Thus, by setting $X_0 = 1$, we consider an upward (positive) bubble, for ease of exposition. Similar results are easily obtained for downward bubbles, conditional on $y_t < y$ where y tends to $-\infty$ with $X_0 = -1$. This result can be applied to the MAR(1,1) and MAR(0,1) processes as follows. Let us first consider the MAR(1,1) process defined in Section 2.1, assuming positive coefficients ϕ and ψ .

Proposition 2: The strictly stationary MAR(1,1) process with i.i.d. errors $\epsilon_t, t = 1, 2, \dots$ from a heavy-tailed distribution with tail index α :

$$(1 - \phi L)(1 - \psi L^{-1})y_t = \epsilon_t,$$

- (i) admits a two-sided MA(∞) representation with the coefficients: $c_h = \frac{1}{1 - \phi\psi} \psi^{-h}$, if $h \leq 0$, and $c_h = \frac{1}{1 - \phi\psi} \phi^h$, if $h \geq 0$.
- (ii) the tail process X_h is such that:

$$X_h = \psi^{-1} X_{h-1} \mathbb{1}_{N \leq -h} + \phi X_{h-1} \mathbb{1}_{N > -h},$$

with $X_0 = 1$, and the probability $P[N = h]$, such that:

$$P[N = h] = \frac{\psi^{-h\alpha}}{\left[\frac{1}{1-\phi^\alpha} + \frac{1}{1-\psi^\alpha} - 1\right]}, \text{ if } h \leq 0,$$

$$P[N = h] = \frac{\phi^{h\alpha}}{\left[\frac{1}{1-\phi^\alpha} + \frac{1}{1-\psi^\alpha} - 1\right]}, \text{ if } h \geq 0,$$

with $0^0 = 1$, by convention.

Proof: See Appendices A1-A2.

We observe that the distribution of variable N is a mixture of two geometric distributions (see Proposition 4).

Corollary 1: In the MAR(1,1) process, we have:

$$X_h = \phi^h \mathbb{1}_{N > \max(-h, 0)} + \phi^{-h-N} \psi^{-N} \mathbb{1}_{0 < N \leq -h} + \phi^{h+N} \psi^N \mathbb{1}_{-h < N \leq 0} + \psi^{-h} \mathbb{1}_{N \leq \min(-h, 0)}$$

Proof: It is done in several steps. First, we solve the backward and forward recursive equations satisfied by the sequences X_h starting from the same initial (terminal) condition X_{-N} . Next, we determine the value of X_{-N} given the known value $X_0 = 1$. In the last step, we combine the results.

(i) It follows from Proposition 2 that for $N > -h$ we have :

$$X_h = \phi X_{h-1}$$

Since $N > -h \iff h > -N \iff h \geq -N + 1$, this leads to a recursive formula with the initial condition X_{-N} and the general term

$$X_h = \phi^{h+N} X_{-N}, \text{ for } h \geq -N + 1$$

(ii) It follows from Proposition 2 that for $N \leq -h$, we have:

$$X_h = \frac{1}{\psi} X_{h-1},$$

which can be written as:

$$X_{h-1} = \psi X_h.$$

Since $N \leq -h \iff -h \geq N \iff h \leq -N$, this leads to a recursive formula with the terminal condition X_{-N} and the general term:

$$X_h = \psi^{-h-N} X_{-N}$$

(iii) These results combined are:

$$X_h = (\phi^{h+N} \mathbb{1}_{N>-h} + \psi^{-h-N} \mathbb{1}_{N \leq -h}) X_{-N}$$

(iv) The value of X_{-N} is unknown and can be determined from $X_0 = 1$ by evaluating the formula above for $h = 0$. We get:

$$\begin{aligned} 1 = X_0 &= (\phi^N \mathbb{1}_{N>0} + \psi^{-N} \mathbb{1}_{N \leq 0}) X_{-N} \\ \iff X_{-N} &= \phi^{-N} \mathbb{1}_{N>0} + \psi^N \mathbb{1}_{N \leq 0} \end{aligned}$$

(v) Next, we compute:

$$\begin{aligned} X_h &= (\phi^{h+N} \mathbb{1}_{N>-h} + \psi^{-h-N} \mathbb{1}_{N \leq -h}) (\phi^{-N} \mathbb{1}_{N>0} + \psi^N \mathbb{1}_{N \leq 0}) \\ &= \phi^h \mathbb{1}_{N>-h} \mathbb{1}_{N>0} + \psi^{-h-N} \phi^{-N} \mathbb{1}_{N \leq -h} \mathbb{1}_{N>0} + \phi^{h+N} \psi^N \mathbb{1}_{N>-h} \mathbb{1}_{N \leq 0} + \psi^{-h} \mathbb{1}_{N \leq -h} \mathbb{1}_{N \leq 0} \\ &= \phi^h \mathbb{1}_{N>Max(-h,0)} + \psi^{-h-N} \phi^{-N} \mathbb{1}_{0 < N \leq -h} + \phi^{h+N} \psi^N \mathbb{1}_{-h < N \leq 0} + \psi^{-h} \mathbb{1}_{N \leq Min(-h,0)} \end{aligned}$$

During a bubble episode, we can distinguish the phases of growth and decline. The non-causal persistence of MAR(1,1) processes determines the rate at which a bubble keeps growing, which is equal to the powers $1/\psi^\alpha, 1/\psi^{2\alpha}, \dots, 1/\psi^{h\alpha}$. The negative power of ψ^α indicates that the growth is explosive up to $t - N$ given that $|\psi| < 1$ is assumed for strict stationarity. The above result is consistent with Proposition 4.2 in [Fries \(2022\)](#) which describes the dynamics of a MAR(1,1) process conditional on a large value $y_t > y$ and $\frac{y_{t+1}}{y_t} = \frac{y_{t+2}}{y_{t+1}} = 1/\psi$. In the MAR(1,1), conditional on $y_t > y$, the bubble either keeps growing to the next value $y_{t+1} = \frac{1}{\psi} y_t$, or it bursts and decreases to $y_{t+1} = \phi y_t$. In a MAR(0,1), the bubble bursts vertically to 0, while in the causal AR(1), i.e., MAR(1,0), we observe a jump, followed by a decrease determined by the autoregressive coefficient, as shown below.

Corollary 2: The strictly stationary MAR(0,1) process with i.i.d. errors $\epsilon_t, t = 1, 2, \dots$ from a heavy-tailed distribution with tail index α :

$$(1 - \psi L^{-1}) y_t = y_t - \psi y_{t+1} = \epsilon_t,$$

admits a one sided MA(∞) representation with the moving average coefficients:

$$c_h = \psi^{-h}, \text{ if } h \leq 0, \text{ and } c_h = 0, \text{ if } h > 0.$$

The tail process is such that

$$X_h = \psi^{-1} X_{h-1} \mathbb{1}_{N \leq -h},$$

with $X_0 = 1$ and the probability $P[N = h]$, such that :

$$\begin{aligned}
P[N = h] &= 0, \text{ if } h > 0, \\
P[N = h] &= (1 - \psi^\alpha)\psi^{-h\alpha}, \text{ if } h \leq 0,
\end{aligned}$$

It follows from Proposition 2 that the variable $-N$ has a geometric distribution on \mathbb{N} with parameter ψ^α during the growth phase of bubble.

The causal autoregressive processes with errors from a heavy-tailed distribution with tail index α may admit a tail process behavior following a jump.

Corollary 3: The strictly autoregressive of order 1 (causal AR(1), i.e. MAR(1,0)) process:

$$y_t = \phi y_{t-1} + \epsilon_t,$$

with i.i.d. errors $\epsilon_t, t = 1, 2, \dots$ from a heavy-tailed distribution with tail index α and $0 < \phi < 1$ admits a one sided MA(∞) with coefficients:

$$c_h = \phi^h \text{ if } h \geq 0, \text{ and } c_h = 0, \text{ if } h < 0.$$

The tail process is such that

$$X_h = \phi X_h \mathbb{1}_{N \geq h},$$

with $X_0 = 1$ and the probability $P[N = h]$, such that :

$$\begin{aligned}
P[N = h] &= 0; \text{ if } h < 0, \\
P[N = h] &= (1 - \phi^\alpha)\phi^{h\alpha}; \text{ if } h \geq 0,
\end{aligned}$$

It follows that the path of y_t displays jumps, with a geometric decline. The variable N has a geometric distribution with parameter ϕ^α during the decline following a jump. Moreover, the behavior of pure noncausal autoregressive processes of order 2 (MAR(0,2) with i.i.d. errors $\epsilon_t, t = 1, 2, \dots$ from a heavy-tailed distribution with tail index α is described in Appendix B.

The results given above suggest the following definition of a bubble:

Definition: The bubble is an episode when the observations above a high threshold on a strictly stationary autoregressive noncausal process with i.i.d. errors from a heavy-tailed distribution with tail index α increase (decline) at the rate of a tail process.

Therefore, at any time t when $y_t > y$ and y is a high threshold it follows from Proposition 1 that the ratios of observations $y_{t+h}/y_t \stackrel{d}{\approx} X_h$ for any h , where $\stackrel{d}{\approx}$ denotes an approximate equality of distributions.

3.2 Tail Behavior of Latent Components

The latent components are defined in equations (3) and (4) as:

$$u_{t+1} = (1 - \phi L)y_{t+1} = y_{t+1} - \phi y_t \text{ and } v_t = (1 - \psi L^{-1})y_t = y_t - \psi y_{t+1}, t = 1, \dots$$

for the MAR(1,1) process. We observe that the ratios of these latent components divided by y_t :

$$\frac{u_{t+h}}{y_t} = \frac{y_{t+h} - \phi y_{t+h-1}}{y_t} \text{ and } \frac{v_{t+h}}{y_t} = \frac{y_{t+h} - \psi y_{t+h+1}}{y_t}$$

are functions of ratios y_{t+h}/y_t for $h \in -H, \dots, H$. Then, we aim at replacing them by the tail components: $U_h = X_h - \phi X_{h-1}$ and $V_h = X_h - \psi X_{h+1}$, respectively. Therefore, when $y_t > y$ is large, they are linear deterministic functions of the components X_h of the tail process.

Let us now examine how Proposition 2 can be used to obtain the asymptotic behavior (in distribution) of some transformations of the series of U_h, V_h , $h = -H, \dots, H$.

Proposition 3: At a time t at which $y_t > y$, a high threshold, we have:

$$u_{t+h}/y_t \stackrel{d}{\approx} X_h - \phi X_{h-1} \equiv U_h, \quad v_{t+h}/y_t \stackrel{d}{\approx} X_h - \psi X_{h+1} \equiv V_h,$$

and

$$U_h = (\psi^{-1} - \phi)X_{h-1}\mathbb{1}_{N \leq -h}, \quad V_h = (1 - \psi\phi)X_h\mathbb{1}_{N > -h-1}.$$

Proof: Let us consider the causal component. It follows from Proposition 2 that:

$$U_h = X_h - \phi X_{h-1} = (\psi^{-1} - \phi)X_{h-1}\mathbb{1}_{N \leq -h}.$$

Similarly, we have:

$$V_h = X_h - \psi X_{h+1} = X_h - X_h\mathbb{1}_{N \leq -h-1} - \psi\phi X_h\mathbb{1}_{N > -h-1} = (1 - \phi\psi)X_h\mathbb{1}_{N > -h-1}.$$

Corollary 4: The causal and noncausal tail components U_h, V_h are such that:

$$\begin{aligned} U_h &= 0, \text{ if } N > -h \Leftrightarrow t + h > t - N, \\ V_h &= 0, \text{ if } N \leq -h - 1 \Leftrightarrow t + h < t - N - 1, \end{aligned}$$

Proposition 3 and Corollary 4 can be interpreted as follows. Let us consider an exogenous time t when $y_t > y$, for large y . Then t is in a bubble episode, with a peak at time $t - N$. The noncausal (resp. causal) tail component is equal to zero after (resp. before) the peak, has the behavior of a MAR(0,1) tail process before the peak (resp. MAR(1,0) tail process after the peak). This result can also be used to determine the behavior of other functions of the causal and noncausal tail components.

Corollary 5: We have

$$\xi_{t,h,k} = \frac{u_{t+h}v_{t+k}}{y_t^2} \stackrel{d}{\approx} U_h V_k = 0, \text{ if } h - k \geq 1.$$

Proof: We see that $U_h V_k = 0 \iff (N > -h) \text{ or } (N \leq -k - 1)$. This condition is equivalent to $N \in \mathbb{Z}$ that is always satisfied iff:

$$\begin{aligned} \mathbb{Z} &= (-\infty, -k - 1] \cup [-h + 1, \infty] \\ &\iff -h + 1 \leq -k - 1 + 1 = -k \\ &\iff h - k \geq 1. \end{aligned}$$

The result follows. In particular, we have:

$$\xi_{t,h} = \frac{u_{t+h+1}v_{t+h}}{y_t^p} \stackrel{d}{\approx} U_{h+1} V_h = 0, \forall h$$

where $p = r + s = 2$ is the combined autoregressive order of the process, and

$$\xi_{t,0} = \frac{u_{t+1}v_t}{y_t^p} \stackrel{d}{\approx} U_1 V_0 = 0.$$

For the MAR(0,1) process with $p = 1$, we get:

(i) at $h = 0$.

$$\xi_{t,0} = \frac{v_t}{y_t} \stackrel{d}{\approx} 1 - \psi X_1,$$

where

$$X_1 = \psi^{-1} \mathbb{1}_{N \leq -1}.$$

The statistic is: $\xi_{t,0} = 1 - \mathbb{1}_{N \leq -1}$ and is always 0 during the bubble.

(ii) at $h = 1$.

$$\xi_{t,1} = \frac{v_{t+1}}{y_t} \stackrel{d}{\approx} X_1 - \psi X_2$$

where

$$X_2 = \psi^{-1} X_1 \mathbb{1}_{N \leq -2}$$

The statistic $\xi_{t,1}$ is equal to 0 as well.

3.3 Time to Peak

Next, we describe the stochastic properties of N , where $t - N$ is interpreted as the time to peak.

Proposition 4: In the MAR(1,1) process, the distribution of N is a mixture of two geometric distributions with $P[N \geq 0] = \frac{1}{1 - \phi^\alpha} / (\frac{1}{1 - \phi^\alpha} + \frac{\psi^\alpha}{1 - \psi^\alpha})$. The distribution of N given $N \geq 0$

is a geometric distribution on \mathbb{N} with parameter ϕ^α , and the distribution of $-1 - N$, given $N \leq -1$ is a geometric distribution on \mathbb{N} with parameter ψ^α .

Proof: From Proposition 2, it follows that:

$$P[N \geq 0] = \frac{1}{1 - \phi^\alpha} / \left(\frac{1}{1 - \phi^\alpha} + \frac{\psi^\alpha}{1 - \psi^\alpha} \right).$$

Then, we have for $h \geq 0$:

$$P(N = h | N \geq 0) = \frac{\phi^{h\alpha}}{1 - \phi^\alpha}, \text{ which is a geometric distribution on } \mathbb{N} \text{ with parameter } \phi^\alpha.$$

For $h < 0$, we have:

$$P(N = h | N < 0) = \frac{\psi^{(-h-1)\alpha}}{1 - \psi^\alpha}, \text{ which means that } -1 - N \text{ has a geometric distribution on } \mathbb{N} \text{ with parameter } \psi^\alpha.$$

Corollary 6: The expected value of N is:

$$E(N) = \frac{1}{\frac{1}{1 - \phi^\alpha} + \frac{1}{1 - \psi^\alpha} - 1} \left(\frac{\phi^\alpha}{(1 - \phi^\alpha)^2} - \frac{\psi^\alpha}{(1 - \psi^\alpha)^2} \right).$$

Proof: We have

$$\begin{aligned} E(N) &= E(N | N \geq 0)P(N \geq 0) + E(N | N \leq -1)P(N \leq -1) \\ &= E(Z_1)P(N \geq 0) + E(-1 - Z_2)P(N \leq -1), \end{aligned}$$

where Z_1, Z_2 follow geometric distributions on \mathbb{N} with parameters ϕ^α and ψ^α , respectively.

It follows that:

$$\begin{aligned} E(N) &= \frac{1}{\frac{1}{1 - \phi^\alpha} + \frac{\psi^\alpha}{1 - \psi^\alpha}} \left[\frac{1}{1 - \phi^\alpha} \frac{\phi^\alpha}{1 - \phi^\alpha} + \frac{\psi^\alpha}{1 - \psi^\alpha} \left(-1 - \frac{\psi^\alpha}{1 - \psi^\alpha} \right) \right] \\ &= \frac{1}{\frac{1}{1 - \phi^\alpha} + \frac{\psi^\alpha}{1 - \psi^\alpha}} \left(\frac{\phi^\alpha}{(1 - \phi^\alpha)^2} - \frac{\psi^\alpha}{(1 - \psi^\alpha)^2} \right). \end{aligned}$$

The expected time to peak, i.e. $(t - N)$ depends on the values of ϕ and ψ and is symmetric in ϕ and ψ . In particular, the expected time to peak is equal to t if $\phi = \psi$, which corresponds to a symmetric bubble. In addition, this expectation depends on α .

It is also interesting to compute the cumulative distribution function (cdf), or survival function of N , to derive the quantiles of the distribution of N and obtain the prediction interval for N . We find the quantiles h_U^* and h_L^* of the distribution of N at levels $(1 - \gamma)$ and γ , where γ is small, which are: h_U^* such that $P[N \leq h_U^*] = \gamma$, and h_L^* such that $P[N > h_L^*] = 1 - \gamma$. By focusing on small γ , we consider separately the geometric distributions of the mixture.

Corollary 7: For $h \leq 0$, sufficiently small, we have:

$$P[N \leq h] = \frac{\psi^{-h\alpha}}{1 - \psi^\alpha} \frac{1}{\left[\frac{1}{1-\phi^\alpha} + \frac{1}{1-\psi^\alpha} - 1\right]},$$

and for $h > 0$, sufficiently large, we have:

$$P[N > h] = \frac{\phi^{h\alpha}}{1 - \phi^\alpha} \frac{1}{\left[\frac{1}{1-\phi^\alpha} + \frac{1}{1-\psi^\alpha} - 1\right]}.$$

Proof: see Appendix.

The expected value (median or mode) provides a point prediction of the time to peak. The quantiles of the distribution of N provide the prediction interval for N .

Example: For the MAR(0,1) process, the variable $-N$ follows a geometric distribution on \mathbb{N} with parameter ψ^α (by Corollary 2, or Proposition 4) during the bubble growth. The cumulative probability function of N is:

$$P[N \leq h] = (1 - \psi^\alpha) \sum_{i \leq h} \psi^{-i\alpha} = (1 - \psi^\alpha) \sum_{i \geq -h} \psi^{i\alpha} = \psi^{-h\alpha},$$

for $h \leq 0$. The mean of this geometric distribution is equal to

$$E(N) = -\frac{1}{1 - \psi^\alpha},$$

and the median is:

$$\text{med}(N) = \left\lfloor \frac{\log 2}{\alpha \log(\psi)} \right\rfloor,$$

or its integer part, and the mode is equal to $\text{mode}(N) = 0$. Since the distribution of $-N$ is skewed, the expectation, median, and mode provide three different point predictions. We illustrate the effect of the parameters ψ and α in Figure 1a.

Up to the effect of the integer part, both the median and expectation are decreasing in ψ^α . To build the prediction interval, we use the quantiles of the geometric distribution, which are determined by inverting the cumulative probability function $P[N \leq h] = \psi^{-h\alpha}$. For a level γ , the quantile is equal to :

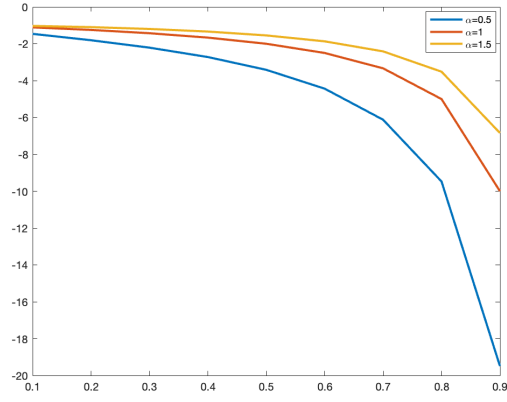
$$h(\gamma) = -\frac{\log \gamma}{\alpha \log \psi}$$

and the prediction interval for N at level 10% is:

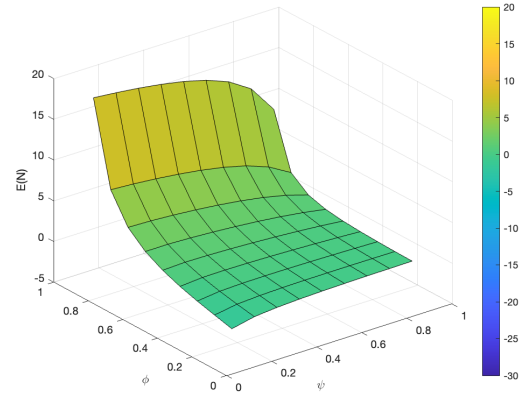
$$\left(-\frac{\log 0.05}{\alpha \log \psi}, -\frac{\log 0.95}{\alpha \log \psi}\right).$$

Because the variable is discrete, we round up or down the upper and lower quantiles to integer values, to make it more conservative. A similar analysis can be applied to the MAR(1,1) process to reveal the effects of ϕ, ψ, α [see, Figure 1].

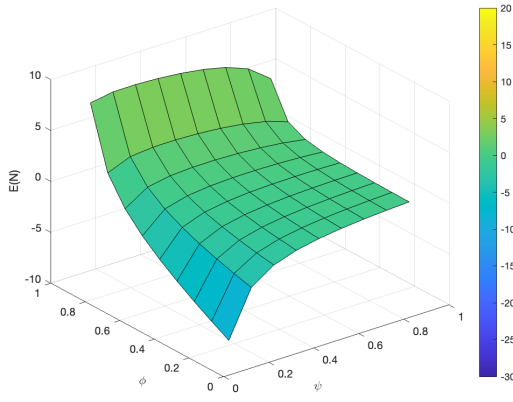
Figure 1: $E(N)$ for $MAR(0,1)$ and $MAR(1,1)$



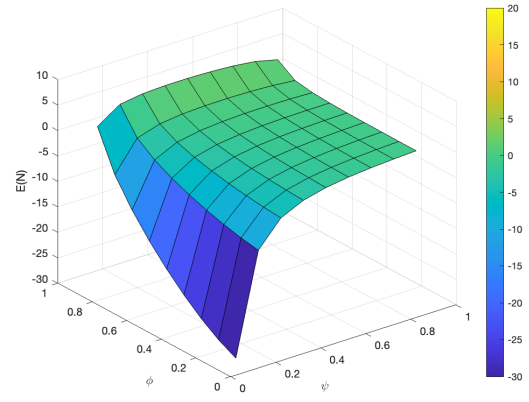
(a) $E(N)$ for $MAR(0,1)$



(b) $E(N)$ for $MAR(1,1)$, $\alpha = 0.5$



(c) $E(N)$ for $MAR(1,1)$, $\alpha = 1$



(d) $E(N)$ for $MAR(1,1)$, $\alpha = 1.5$

4 Inference

4.1 The Statistics

Let us show how the results derived in the previous section can be used to build diagnostic tools for testing the MAR(1,1) process for bubbles. The diagnostics are based on the sample counterparts of

$$\xi_{t,0} = \frac{u_{t+1}v_t}{y_t^2} = \left(\frac{y_{t+1}}{y_t} - \phi_0 \right) \left(1 - \psi_0 \frac{y_{t+1}}{y_t} \right),$$

where ϕ_0, ψ_0 denote the true values of the parameters. These quantities depend on the observations and the unknown parameters. The unknown parameters can be replaced by consistent and asymptotically normally distributed estimators $\hat{\phi}_T, \hat{\psi}_T$ of ϕ, ψ obtained from the sample of T observations. Then, the sample counterpart of $\xi_{t,0}$ is:

$$\hat{\xi}_{t,T} = \left(\frac{y_{t+1}}{y_t} - \hat{\phi}_T \right) \left(1 - \hat{\psi}_T \frac{y_{t+1}}{y_t} \right).$$

The statistics $\hat{\xi}_{t,T}, t = 1, \dots, T$ can be used as follows. From Corollary 5, we know that if y_t is sufficiently large at time t , then $\xi_t \stackrel{d}{\approx} U_1 V_0$ and that $U_1 V_0 = 0$. Therefore, at such a t we expect that $\hat{\xi}_{t,T}$ is close to 0. We can also consider another lag h with:

$$\xi_t(h) = \frac{u_{t+h+1}v_{t+h}}{y_t^2} = \left(\frac{y_{t+h+1}}{y_t} - \phi_0 \frac{y_{t+h}}{y_t} \right) \left(\frac{y_{t+h}}{y_t} - \psi_0 \frac{y_{t+h+1}}{y_t} \right).$$

It was shown in Corollary 5 that $\xi_{t,h} \stackrel{d}{\approx} U_{h+1} V_h$ and that $U_{h+1} V_h = 0$. The sample counterpart is:

$$\hat{\xi}_{t,T}(h) = \frac{\hat{u}_{t+h+1}\hat{v}_{t+h}}{y_t^2} = \left(\frac{y_{t+h+1}}{y_t} - \hat{\phi}_T \frac{y_{t+h}}{y_t} \right) \left(\frac{y_{t+h}}{y_t} - \hat{\psi}_T \frac{y_{t+h+1}}{y_t} \right).$$

4.2 Confidence Band

Let us consider the statistic $\hat{\xi}_{t,T}$. The zero value of the transformed tail process can be considered as the true value of some tail parameter $\theta_1 = U_1 V_0$, which is deterministic and equal to 0 if y_t is sufficiently large, and it is stochastic, otherwise. Then, at each exogenous time t , we can consider the null hypothesis:

$$H_{0,1} = \{\theta_1 = 0\}.$$

The difficulty is that we have a double asymptotic in the level of threshold y and in the number of observations T . To derive reliable confidence bands, we assume that at the times t of the bubble, the uncertainty in the approximation $\xi_{t,0} \stackrel{d}{\approx} U_1 V_0$ is negligible with respect

to the asymptotic in T . Then, at time t corresponding to a bubble episode when $H_{0,1}$ is satisfied and $y_t > y$, with large y , we have conditional on y_t, y_{t+1} :

$$\begin{aligned} \sqrt{T}(\hat{\xi}_{t,T} - \xi_{t,0}) &\stackrel{d}{=} \sqrt{T}(\hat{\xi}_{t,T} - U_1 V_0) \\ &= \sqrt{T}\hat{\xi}_{t,T} \xrightarrow{d} N(0, \sigma_t^2), \end{aligned}$$

where σ_t^2 is obtained by the delta method. We have:

$$\sigma_t^2 = V_t \left\{ \left[- \left(1 - \psi_0 \frac{y_{t+1}}{y_t} \right), \frac{-y_{t+1}}{y_t} \left(\frac{y_{t+1}}{y_t} - \phi_0 \right) \right] \sqrt{T} \begin{pmatrix} \hat{\phi}_T - \phi_0 \\ \hat{\psi}_T - \psi_0 \end{pmatrix} \right\}.$$

This quantity is then consistently estimated from:

$$\hat{\sigma}_{t,T}^2 = \left(\frac{\hat{v}_t}{y_t}, \frac{y_{t+1}\hat{u}_{t+1}}{y_t^2} \right) \hat{\Omega}_T \begin{pmatrix} \frac{\hat{v}_t}{y_t} \\ \frac{y_{t+1}\hat{u}_{t+1}}{y_t^2} \end{pmatrix},$$

where $\hat{\Omega}_T$ is a consistent estimator of the asymptotic variance matrix of the parameter estimators. Then, under the assumption of a MAR(1,1) process and at times t such that y_t is sufficiently large, we have:

$$|\sqrt{T}\hat{\xi}_{t,T}/\hat{\sigma}_{t,T}| \leq 1.96,$$

with the asymptotic probability of 95 %. This leads to a functional diagnostic tool that consists of reporting for any time t the quantities $\hat{\xi}_{t,T}$, $t = 1, \dots, T$ along with the band

$$\left(\hat{\xi}_{t,T} \pm 1.96 \frac{\hat{\sigma}_{t,T}}{\sqrt{T}} \right).$$

Since the tail process does not depend on the level of y_t and the values of y_{t+1} , the width of the band is independent of time t , $t = 1, \dots, T$. Then, the times t at which the statistic is inside the band are the times associated with a bubble with probability 95 %.

This approach is easily extended to other lags. From the statistic $\hat{\xi}_{t,T}(h)$, we can test the null hypothesis:

$$H_{0,h} = \{\theta_h = 0\}$$

where $\theta_h = U_{h+1}V_h$ and $y_t > y$. Then, conditional on y_t, y_{t+h}, y_{t+h+1} we have:

$$\begin{aligned} \sqrt{T}(\hat{\xi}_{t,T}(h) - \xi_{t,h}) &\stackrel{d}{=} \sqrt{T}(\hat{\xi}_{t,T}(h) - U_{h+1}V_h) \\ &= \sqrt{T}\hat{\xi}_{t,T}(h) \xrightarrow{d} N(0, \sigma_t^2(h)) \end{aligned}$$

where $\sigma_t^2(h)$ is:

$$\sigma_t^2(h) = V_t \left\{ \left[\frac{-y_{t+h}}{y_t} \left(\frac{y_{t+h}}{y_t} - \psi_0 \frac{y_{t+h+1}}{y_t} \right), \frac{-y_{t+h+1}}{y_t} \left(\frac{y_{t+h+1}}{y_t} - \phi_0 \frac{y_{t+h}}{y_t} \right) \right] \sqrt{T} \begin{pmatrix} \hat{\phi}_T - \phi_0 \\ \hat{\psi}_T - \psi_0 \end{pmatrix} \right\}.$$

This quantity is then consistently estimated from:

$$\hat{\sigma}_{t,T}^2(h) = \left(\frac{y_{t+h}\hat{v}_{t+h}}{y_t^2}, \frac{y_{t+h+1}\hat{u}_{t+h+1}}{y_t^2} \right) \hat{\Omega}_T \begin{pmatrix} \frac{y_{t+h}\hat{v}_{t+h}}{y_t^2} \\ \frac{y_{t+h+1}\hat{u}_{t+h+1}}{y_t^2} \end{pmatrix}.$$

Under the assumption of a MAR(1,1) process and at times t such that $y_t > y$ is sufficiently large:

$$|\sqrt{T} \hat{\xi}_{t,T}(h) / \hat{\sigma}_{t,T}(h)| \leq 1.96,$$

with the asymptotic probability of 95 %. This leads to a set of functional diagnostic tools, where for any time t and h the quantities $\hat{\xi}_{t,T}(h)$, $t = 1, \dots, T$ are reported along with the band:

$$\left(\hat{\xi}_{t,T}(h) \pm 1.96 \frac{\hat{\sigma}_{t,T}(h)}{\sqrt{T}} \right).$$

It is important to note that the above procedure does not distinguish between a bubble and a short-lasting spike. In addition, there can be bubble times t when the statistic is outside the band because (i) the MAR(1,1) model is misspecified, or (ii) the MAR(1,1) is well specified, but the level of y_t is not sufficiently large.

The specific approaches for MAR(1,0) and MAR(0,1) processes are obtained easily from this method. The above results can be generalized to the MAR(0,1) process or used for jump detection in the causal MAR(1,0) process. The confidence bands are independent of the tail parameter α . The tail parameter α can be approximated by the Hill estimator, which suffers from the bias-variance trade-off in the finite sample. [Kulik and Soulier \(2020\)](#) shows that under the tail process approach, the Hill estimator is consistent and asymptotically normally distributed.

The confidence bands are independent of the tail parameter α . The tail parameter α can be approximated by the Hill estimator, which suffers from the bias-variance trade-off in the finite sample. [Kulik and Soulier \(2020\)](#) shows that under the tail process approach, the Hill estimator is consistent and asymptotically normally distributed. $\hat{\xi}_{t,T}$ can be used as a tool of bubble detection in the MAR(1,1) and MAR(0,1) processes, as it is constant and close to 0 both during the bubble growth and decline periods, and it is time-varying otherwise [see Appendix C]. Hence, the first difference $\Delta \hat{\xi}_{t,0}$ is also constant and close to 0 during the bubble growth and decline periods.

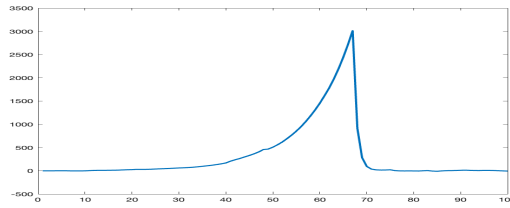
Let us consider a sequence of $\hat{\xi}_{t,T}$ evaluated at $t=1,2,\dots$ following a large threshold value y_t . A close to zero value of $\hat{\xi}_{t+1,T}$ following a large value y_t is a warning of an upcoming

bubble. Since this statistic remains close to 0 over the entire duration of the bubble, the number of statistically non-significant values of $\xi_t(1)$, for $t = t + 1, t + 2, \dots$ is a measure of bubble duration. The first time t_j when $\hat{\xi}_{t_j,T} \approx 0$ marks the start of the bubble. The last time t_J , such that $\hat{\xi}_{t_J,T}(1) \approx 0$ marks the end of the bubble.

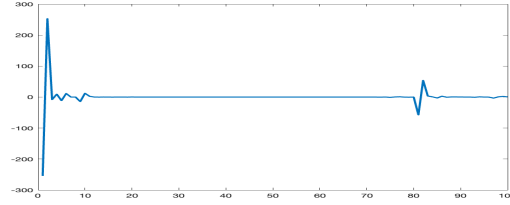
4.3 Illustration

Our approach is illustrated in Figure 2 by a bubble episode of a simulated MAR(1,1) process with $\psi = 0.9, \phi = 0.3$ and Cauchy distributed errors with scale coefficient 1.

Figure 2: Bubble detection in MAR(1,1) process



(a) MAR(1,1) process



(b) Path of $\Delta\xi_t$

The top panel of the Figure displays the bubble episode of the MAR(1,1) process. The first difference $\Delta\hat{\xi}_t$ of statistic

$$\Delta\hat{\xi}_t = \Delta \frac{\widehat{icov}_{t,1}(u, v)}{y_t^2}, \quad y_t \neq 0$$

is computed and displayed graphically to detect the periods when it is approximately constant and close to 0. The statistic $\Delta\hat{\xi}_t$ indicates the times when the process becomes a "tail process", which can be used to approximate the start and end of a bubble. The bottom panel shows the first difference $\Delta\xi_t$. The first difference $\Delta\xi_t$ is constant and close to zero during the entire bubble episode.

5 Green Stock Indexes and ETFs

The transition to a clean energy economy has recently gained significant attention, driven by global events such as the COVID-19 pandemic and the Russia-Ukraine war. Indeed, in response to these crises, governments, industries, and investors have increasingly prioritized clean energy investments, recognizing their long-term benefits for a stable and environmentally friendly energy system [Mohammed et al. (2023)]. This growing focus on clean energy is also driven by the need to achieve net-zero emissions by 2050, which requires substantial investment in clean energy from both developed and developing countries; see Khalifa et al. (2022). In 2023, global investment in the energy sector was estimated at USD 2.8 trillion, an increase of 0.6 trillion USD from five years earlier. Almost all of this growth was directed toward clean energy and infrastructure, increasing total clean energy spending to 1.8 trillion USD, compared to 1 trillion USD for fossil fuels.⁵ These large investments pose the risk of "green bubbles" – rapid stock price increases followed by crashes. Specifically, such bubbles occur when over-investment and speculative behavior drive the market value of clean energy assets beyond sustainable levels. Consequently, rising interest rates can increase financial pressure on investors, potentially triggering bubble bursts and undermining the credibility of the clean energy transition [Wimmer (2016)].

5.1 The Data

We have considered the Renixx Index, the WHETF and the iShare green stock ETFs. For Renixx, we used daily data from <https://www.renewable-energy-industry.com/stocks> and sampled them at a monthly frequency by taking the last day of each month of the closing price series. When the last day of the month is a bank holiday, we consider the previous available day. The Renixx index tracks the global renewable energy market, covering sectors such as wind, solar, bioenergy, geothermal, hydropower, electronic mobility, and fuel cells. It comprises 30 companies, each of which derives more than 50% of its revenues from these sectors (see www.iwr.de/renixx). The WHETF tracks the WilderHill Clean Energy ETF, which includes companies listed in the United States that focus on developing cleaner energy and conservation efforts. In particular, WHETF allocates a minimum of 90% of its total assets to common stocks included in this ETF. It is rebalanced and reconstituted quarterly. Finally, iShare tracks the S&P Global Clean Energy ETF, which provides exposure to the 30 largest and most liquid publicly traded companies worldwide that operate in the clean

⁵IEA (2023), World Energy Outlook 2023, IEA, Paris <https://www.iea.org/reports/world-energy-outlook-2023>, Licence: CC BY 4.0 (report); CC BY NC SA 4.0 (Annex A).

energy sector. The latter uses a modified market capitalization weighting system.

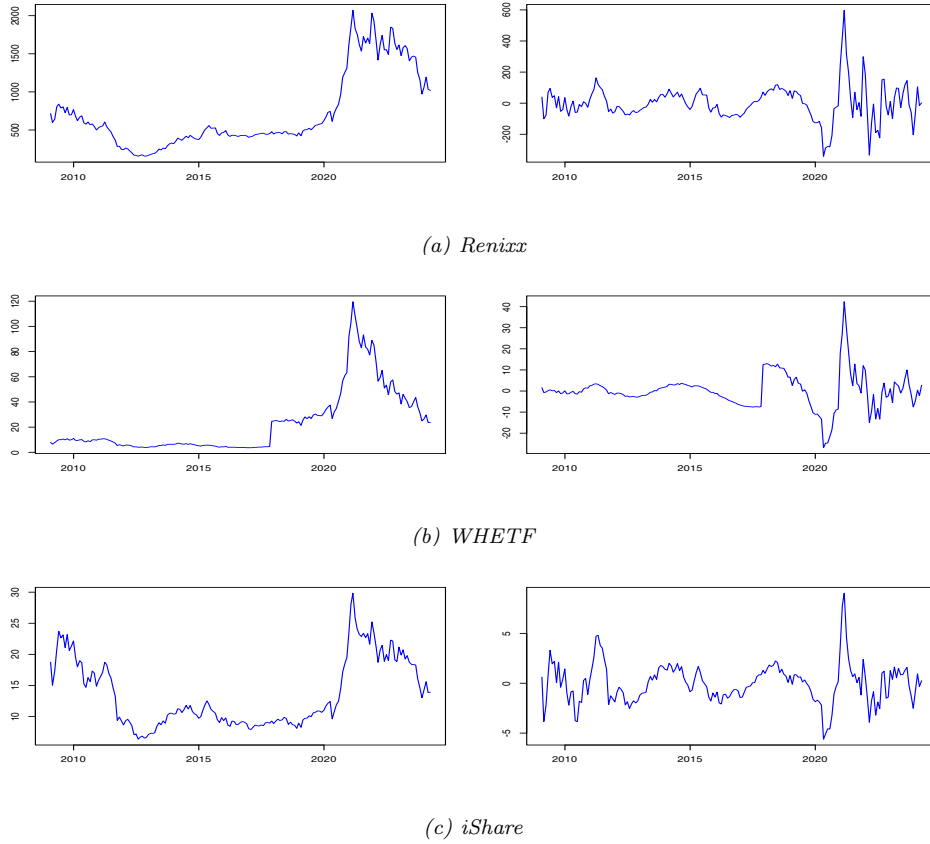
We investigate the Renixx on its whole available sample and both WHETF and iShare from 2009 onward to avoid the latter two ETFs starting the sample in the middle of the financial bubble. We consequently have a total of $T = 266$ observations for Renixx and $T = 182$ observations for WHETF and iShare, with potentially two bubble patterns for Renixx and a single bubble for both the WHETF and iShare. Figure 3a shows that the Renixx index (from January 2002 to February 2024) experienced significant bubbles in 2008 and 2020, coinciding with two major global events: the 2008 financial crisis and the outbreak of the COVID-19 pandemic. In 2008, the financial crisis rocked global markets, leading to widespread economic instability and investor panic. The collapse of major financial institutions, coupled with a credit crunch and falling stock markets, triggered a flight to safety among investors. This risk aversion had a significant impact on the renewable energy sector, with reduced investment in renewable energy projects and falling demand for renewable energy stocks [see Giorgis et al. (2024)]. Similarly, in 2020, the COVID-19 pandemic caused unprecedented economic disruption around the world. Lockdown measures, supply chain disruptions, and reduced consumer spending resulted in a global economic downturn. The renewable energy sector was particularly affected by the decrease in energy demand due to reduced economic activity and travel restrictions. The same trends are observed in WETHF and iShare; Figures 3b and 3c, respectively. However, only the COVID period bubble appears in the data, as the sample for both variables spans from January 2009 to February 2024, and therefore does not include data from the global financial crisis.

5.2 Prices vs. Returns

While most studies in green energy finance focus on returns [e.g., Henriques and Sadorsky (2008); Sadorsky (2012)], our analysis is based on prices, allowing for a direct examination of bubble dynamics that would otherwise be obscured by log-differencing. Indeed, in financial analysis, especially in commodity pricing, it is crucial to focus on the price process rather than returns or first differences. This approach aligns with the financial theory that underlies commodity pricing, as discussed in Hull and Basu (2016). Transforming the price series into returns or first differences can obscure critical aspects of the price process, including the presence of bubbles. Moreover, differencing can eliminate noncausal components essential for understanding bubble dynamics [Giancaterini et al. (2022)]. We employ the detrended cubic spline method to address this issue and eliminate trend components while preserving significant bubble patterns, as detailed in Hall and Jasiak (2024). This method fits a cubic

spline, a piecewise function composed of polynomial segments of degree three, to the time series data. The points where these segments connect, known as knots, allow separate cubic polynomials to be fitted within each segment. We place knots every two years to effectively detrend the series, balancing data smoothing and avoiding overfitting. By applying this approach, we successfully isolate the cyclical variations that contain the bubble patterns from the trend component. The detrended series are also shown in the right panels of Figure 3.⁶

Figure 3: Green Index and ETFs from January 2009 to February 2024. The panels on the left show the original series, while those on the right display their detrended versions.



⁶An alternative detrending technique that may help us preserve the bubble patterns is the HP filter method (see [Giancaterini et al. \(2022\)](#), [Hecq and Voisin \(2023\)](#)). However, as indicated by [Hall and Jasiak \(2024\)](#), the HP filter requires you to choose a value for the smooth parameter lambda, which is typically a function that increases with the sampling frequency of the data. In our examination of monthly data, a high lambda value may result in computational inaccuracies, thus justifying our preference for using a cubic spline to detrend the data. We have nevertheless investigated several detrending methods, including the HP filter, as well as polynomial trends of different degrees (results upon request). We only report the outcomes with the spline detrending approach as it is the only one that passes the i.i.d. test introduced in [Jasiak and Neyazi \(2023\)](#) on the detrended series.

5.3 Summary Statistics and MAR Estimations

Table 1 presents the summary statistics, which further confirm the non-Gaussian nature of the series. We test the spline-detrended data for causal and noncausal persistence by using the test introduced in Jasiak and Neyazi (2023) [see Section 2.2]. We choose $K = 2$, including time series and the square of it as (non)linear transformations, and $H = 3$ as a number of lags included in the covariance matrix in the objective function of the test. The critical value at a 5% significance level from the Chi-square distribution $\chi^2(12) = 21.026$, and it becomes clear that the null hypothesis of the absence of nonlinear serial dependence is rejected since the test value is 514.98. This means that we reject the null hypothesis i.i.d. for the sole series detrended, and an extension of the model to improve the dynamics is required.

Table 1: Summary statistics of Renixx, WHETF, and iShare

	T	Mean	Min	Max	SD	Skewness	Kurtosis
Renixx	266	748.57	155.47	2070.38	475.09	1.03	2.85
WHETF	182	23.08	3.66	119.57	25.31	1.67	5.28
iShare	182	13.60	6.36	29.83	5.46	0.74	2.36

We next apply the GCov estimation method to estimate the three green indicators. Specifically, we set the parameters $H = K = 2$ and choose $a_j(\epsilon_t) = \epsilon_t^j$, for $j = 1, 2$, in (5). In other words, we use the residuals and their squares as transformations in the estimation process; see Cubadda et al. (2023). To identify the dynamics of the underlying processes, we evaluate all combinations of r and s such that $r + s = p$. We begin with $p = 1$ and gradually increase p , stopping when we find the values of r and s that provide residuals i.i.d.. This approach allows us to identify the one index and two ETFs as MAR(1, 1). However, when estimating WHETF and iShare, we find that $\Gamma(0, \hat{\theta})^{-1}$ in (5) has coefficients very close to zero, with causal and noncausal parameters approaching unity, indicating large variance in residuals. Consequently, we believe that using powers of the residuals as nonlinear functions is not optimal for these series, as it further amplifies the large variances and may lead to computational issues. Instead, we opt for $a_j(\epsilon_t) = \log(|ps|)^j$ for $j = 1, 2$, as this logarithmic transformation helps mitigate the computational problems associated with these variances. Table 2 presents the results using $a_j(\epsilon_t) = \epsilon_t^j$ (with $j = 1, 2$) for Renixx, while $a_j(\epsilon_t) = \log(|ps|)^j$ for WHETF and iShare. The last row of the Table shows the results of the GCov test. The test results indicate that the processes are correctly specified and provide a good fit to the data.

Figure 4: Causal and noncausal components

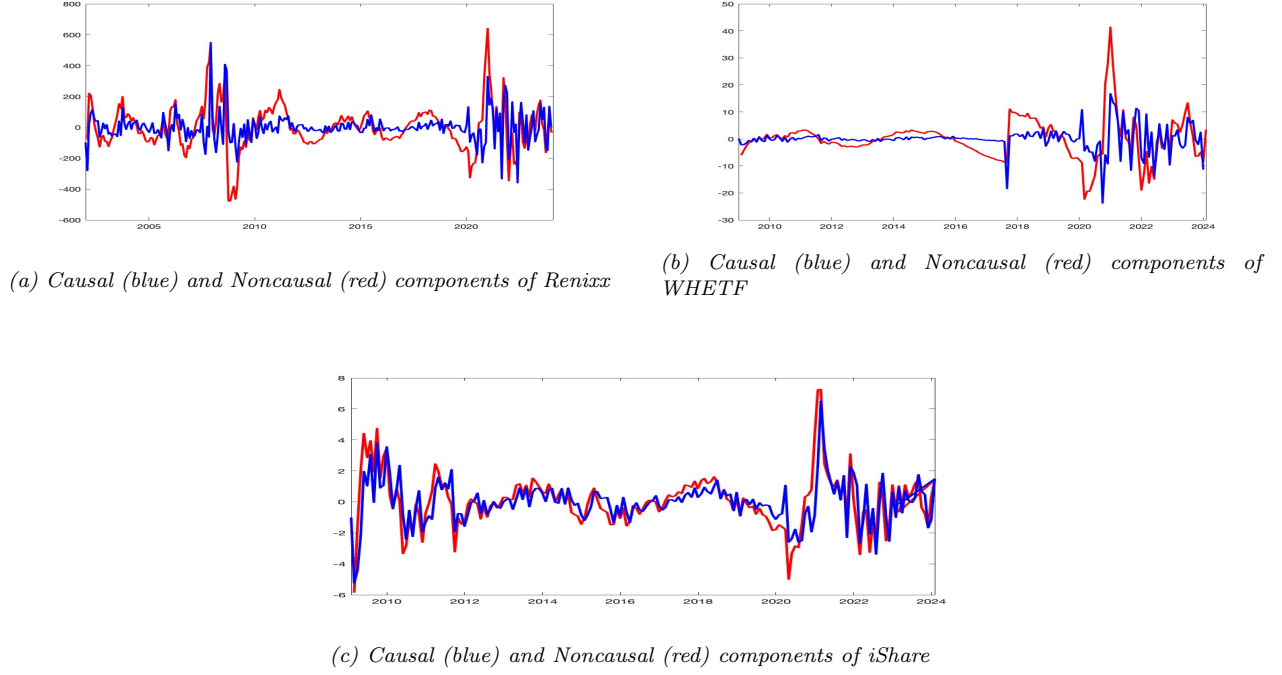


Table 2: Estimated $MAR(1,1)$ coefficients and $GCov$ tests

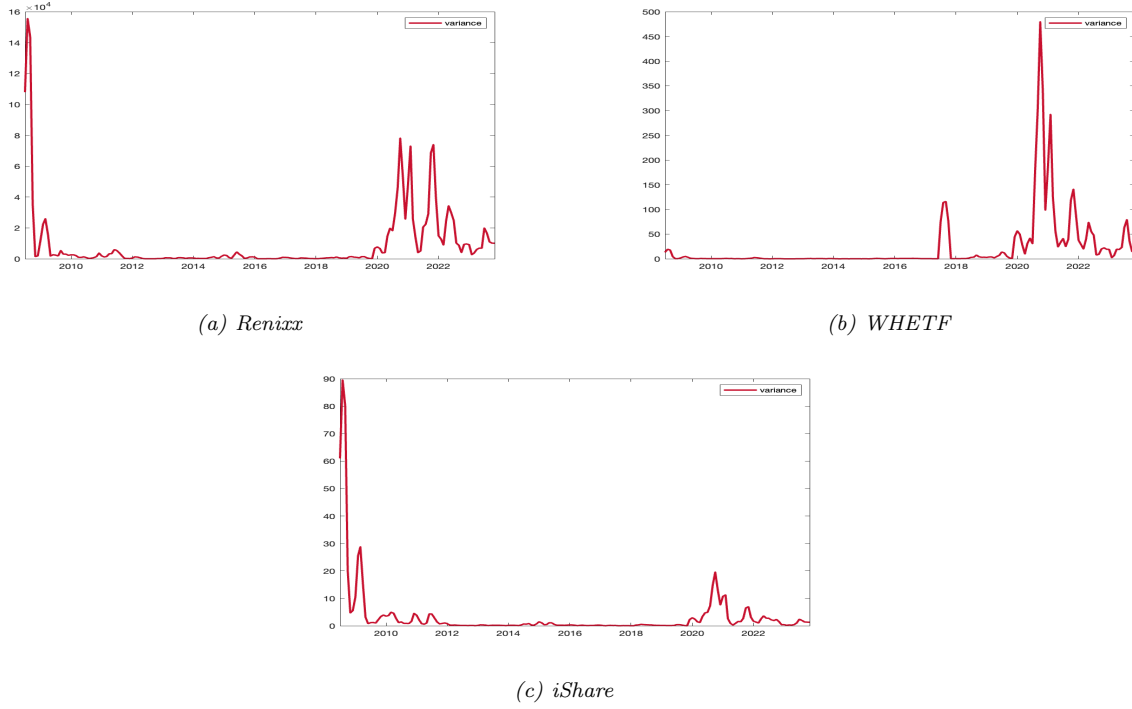
$MAR(1,1)$	Renixx	WHETF	iShare
ϕ	0.24 (0.11)	0.07 (0.01)	0.32 (0.02)
ψ	0.70 (0.08)	0.89 (0.03)	0.62 (0.02)
$GCov$ Test (Critical Value)	7.14 (12.59)	4.86 (12.59)	2.40 (12.59)

5.4 Bubble Detection

First, we estimate local variance to detect the periods with high volatility. We consider a rolling window of 5 observations and estimate the local variance for all three series. Figure 5 displays the rolling estimates of the conditional variances of the Renixx index and two ETFs. Two bubble periods, one that occurred during the financial crisis of 2008 and one associated with the COVID pandemic, are observable in Figure 5. Since the available data on ETFs is limited during the first bubble period, we focus on the second bubble period only. This approach is clearly an alternative to time-varying unit root tests that are frequently used in

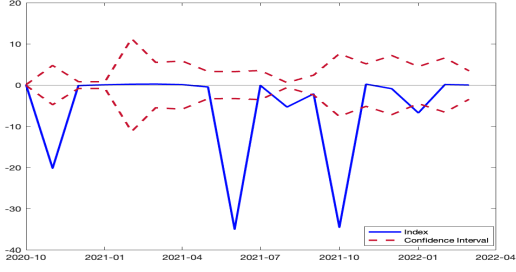
the literature.

Figure 5: Local variance of time series with $H = 5$ rolling window size

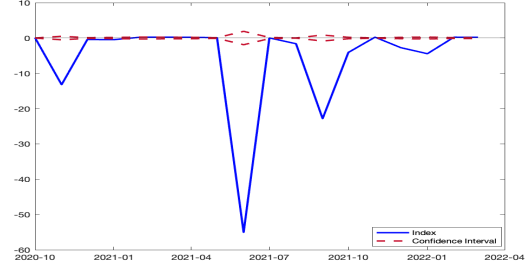


Next, to detect and determine the number of bubbles in the second period of bubbles, we focus specifically on the period between 12/01/2020 and 05/31/2021. Figure 6 illustrates how the method introduced in Section 3 can be applied to Rennix and other ETFs to detect the bubble and to determine the dates at which that bubble starts and ends. Figure 6a and 6b show that the second bubble of Rennix and WTETF started on 12/01/2020 and ended on 03/01/2021. The first bubble for ishare ended on 04/30/2021; however, in Figure 6c is not evident since the confidence interval is narrow, since the variance of the parameters as reported in Table 2 is higher than the other estimated parameters, and it shrinks the confidence interval.

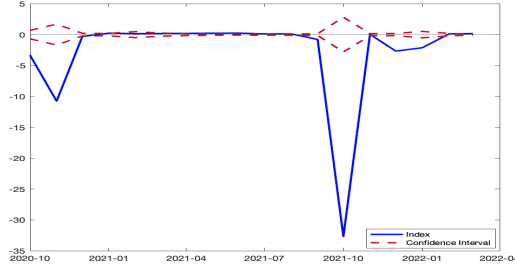
Figure 6: Bubble detection statistics for Renixx, WHETF, and ishare



(a) Renixx



(b) WHETF



(c) iShare

6 Conclusions

This paper studies bubble phenomena in the green sector by using mixed causal and non-causal models. Our method of bubble detection is based on strictly stationary noncausal processes and their tail process representation during a bubble. Specifically, by using univariate $MAR(r, s)$, it analyzes one key index and two Key ETFs, namely the Renixx index, WHETF, and iShare, and finds that a bubble pattern characterizes all three variables.

A Appendix A

1. Derivation of the MA(∞) representation of MAR(1,1)

We have:

$$(1 - \phi L)(1 - \psi L^{-1}) = -\psi L^{-1}(1 - \phi L)(1 - \psi^{-1}L).$$

It follows using the partial fraction decomposition of the polynomial that:

$$\begin{aligned} \frac{1}{(1 - \phi L)(1 - \psi L^{-1})} &= -\psi^{-1}L \frac{1}{(1 - \phi L)(1 - \psi^{-1}L)} \\ &= \frac{-\psi^{-1}L}{\phi - \psi^{-1}} \left(\frac{\phi}{1 - \phi L} - \frac{\psi^{-1}}{1 - \psi^{-1}L} \right) \\ &= \frac{1}{1 - \phi\psi} \left(\frac{\phi L}{1 - \phi L} - \frac{\psi^{-1}L}{1 - \psi^{-1}L} \right) \\ &= \frac{1}{1 - \phi\psi} \left(\frac{\phi L}{1 - \phi L} + \frac{1}{1 - \psi L^{-1}} \right) \\ &= \frac{1}{1 - \phi\psi} \left(\sum_{h=1}^{\infty} \phi^h L^h + \sum_{h=0}^{\infty} \psi^h L^{-h} \right) \\ &= \frac{1}{1 - \phi\psi} \left(\sum_{h=1}^{\infty} \phi^h L^h + \sum_{h=0}^{-\infty} \psi^{-h} L^h \right), \end{aligned}$$

where we observe that the first sum inside the brackets is equal to $\frac{1}{1 - \phi L} - 1$, and the second sum is equal to $\frac{1}{1 - \psi L^{-1}}$. The moving average coefficients are:

$$c_h = \frac{\phi^h}{1 - \phi\psi}, \text{ if } h > 0, \quad \text{and} \quad c_h = \frac{\psi^{-h}}{1 - \phi\psi}, \text{ if } h \leq 0,$$

since the two formulas coincide for $h = 0$ and the convention $0^0 = 1$ is used (if ϕ or ψ is zero).

2. Proof of Proposition 2:

The tail process takes the values either $1/\psi X_{h-1}$, or ϕX_{h-1} . Then, we have:

$$\text{a) if } N + h \leq 0 \iff N \leq -h : X_h = \frac{1}{1 - \phi\psi} \psi^{-N-h} / \frac{1}{1 - \phi\psi} \psi^{-N-h-1} X_{h-1} = \psi^{-1} X_{h-1},$$

$$\text{b) if } N + h > 0 \iff N > -h : X_h = \frac{1}{1 - \phi\psi} \phi^{N+h} / \frac{1}{1 - \phi\psi} \phi^{N+h-1} X_{h-1} = \phi X_{h-1},$$

with $X_0 = 1$.

Then, the probability distribution of N is such that :

$$P[N = h] = \frac{(1 - \phi\psi)^{-1} \psi^{-h\alpha}}{(1 - \phi\psi)^{-1} [\frac{1}{1 - \phi^\alpha} + \frac{1}{1 - \psi^\alpha} - 1]} = \frac{\psi^{-h\alpha}}{[\frac{1}{1 - \phi^\alpha} + \frac{1}{1 - \psi^\alpha} - 1]}; \text{ if } h \leq 0,$$

$$P[N = h] = \frac{(1 - \phi\psi)^{-1} \phi^{h\alpha}}{(1 - \phi\psi)^{-1} [\frac{1}{1 - \phi^\alpha} + \frac{1}{1 - \psi^\alpha} - 1]} = \frac{\phi^{h\alpha}}{[\frac{1}{1 - \phi^\alpha} + \frac{1}{1 - \psi^\alpha} - 1]}; \text{ if } h \geq 0,$$

with $0^0 = 1$, by convention.

3. Tail process representation of AR(2) processes with at least one root inside the unit circle

The autoregressive of order 2, AR(2), process:

$$y_t = t_1 y_{t-1} + t_2 y_{t-2} + \epsilon_t \Rightarrow y_t(1 - t_1 L - t_2 L^2) = \epsilon_t$$

with i.i.d. errors $\epsilon_t, t = 1, 2, \dots$ from a heavy-tailed distribution with tail index α can admit a tail process behavior. We distinguish the following cases:

a) $1 - t_1 L - t_2 L^2 = (1 - \lambda_1 L)(1 - \lambda_2 L)$, the root reciprocals λ_1 and λ_2 are real, distinct, and such that either λ_1 and λ_2 are real, distinct, and such that either $|\lambda_1| < 1$ and $|\lambda_2| < 1$ (causal process), or $|\lambda_1| > 1$ and $|\lambda_2| > 1$ (noncausal process). Then, the process can be written as a strictly stationary pure either causal, or noncausal process.

The causal process admits a one-sided MA(∞) representation with the coefficients $c_h = \frac{1}{\lambda_1 + \lambda_2}[(\lambda_2)^h + (\lambda_1)^h]$, for $h \geq 0$. The noncausal process admits a one-sided MA(∞) representation with the coefficients $c_h = \frac{1}{\lambda_1 - \lambda_2}[(\lambda_2)^{h+1} - (\lambda_1)^{h+1}]$, for $h \leq 0$

b) $1 - t_1 L - t_2 L^2 = (1 - \lambda L)^2$, the root reciprocal λ is real and such that either $|\lambda| < 1$ (double causal root), or $|\lambda| > 1$ (double noncausal root). This case does not satisfy the geometric ergodicity condition and is excluded.

d) $1 - t_1 L - t_2 L^2 = (1 - \lambda_1 L)(a - \lambda_2 L)$, the roots $1/\lambda_1$ and $1/\lambda_2$ are imaginary and equal to a pair of complex conjugates of modulus greater than 1. This case is excluded as it results in local explosive oscillations, while a bubble requires local explosive growth.

4. Comparison with Fries (2022) For illustration, let us consider $h = 0$ and the MAR(1,1) process with α -stable distributed errors using the approach of Fries (2022). It follows from Propositions 1 and 2 that, conditional on a bubble onset at time t and large $y_t > y$ we have:

$$\begin{aligned} E\left(\frac{u_{t+1}v_t}{y_t^2} | y_t > y\right) &= E\left(\left(\frac{y_{t+1} - \phi y_t}{y_t}\right)\left(\frac{y_t - \psi y_{t+1}}{y_t}\right) | y_t > y\right) \\ &\approx E((X_1 - \phi)(1 - \psi X_1)) \\ &= p^+ (\psi^{-1} - \phi) (1 - \psi \psi^{-1}) + p^- (\phi - \phi) (1 - \psi \phi) \\ &= 0 \end{aligned}$$

where we replace $\frac{y_t}{y_t}$ by $X_0 = 1$, $\frac{y_{t+1}}{y_t}$ by X_1 , independent of t and y , and the probabilities p^+ and p^- for $h \leq -1$ and $h \geq 0$, of bubble growth and burst, respectively, are defined in Proposition 2.

Let us consider $h = 0$ and the MAR(0,1) process. In this process, component $u_t = 1$ and only the component v_t is relevant. Hence, conditional on the bubble onset at time t for large $y_t > y$ we have:

$$\begin{aligned} E\left(\frac{u_{t+1}v_t}{y_t} | y_t > y\right) &= E\left(\left(\frac{y_t - \psi y_{t+1}}{y_t}\right) | y_t > y\right) \\ &\approx E(1 - \psi X_1) \\ &= p^+ (1 - \psi \psi^{-1}) \\ &= 0, \end{aligned}$$

where we replace $\frac{y_{t+1}}{y_t}$ by X_1 , independent of t and y , $\frac{y_t}{y_t} = X_0 = 1$ and the probability p^+ of bubble growth is given in Corollary 2.

5. The cumulative probability distribution of N

a) For the MAR(1,1) process:

If $h < 0$, we have:

$$\begin{aligned} P[N \leq h] &= \sum_{i \leq h} \frac{\psi^{-i\alpha}}{\left[\frac{1}{1-\phi^\alpha} + \frac{1}{1-\psi^\alpha} - 1\right]} \\ &= \sum_{i \geq -h} \frac{\psi^{i\alpha}}{\left[\frac{1}{1-\phi^\alpha} + \frac{1}{1-\psi^\alpha} - 1\right]} \\ &= \frac{\psi^{-h\alpha}}{1 - \psi^\alpha} \frac{1}{\left[\frac{1}{1-\phi^\alpha} + \frac{1}{1-\psi^\alpha} - 1\right]} \end{aligned}$$

If $h > 0$, then:

$$P[N > h] = \frac{\phi^{h\alpha}}{1 - \phi^\alpha} \frac{1}{\left[\frac{1}{1-\phi^\alpha} + \frac{1}{1-\psi^\alpha} - 1\right]}$$

b) For the MAR(0,1) process with $N \leq 0$ and $h \leq 0$, we have:

$$P[N \leq h] = (1 - \psi^\alpha) \sum_{i \leq h} \psi^{-i\alpha} = (1 - \psi^\alpha) \sum_{i \geq -h} \psi^{i\alpha} = \psi^{-h\alpha}$$

.

References

- Basrak, B. and J. Segers (2009). Regularly varying multivariate time series. *Stochastic processes and their applications* 119(4), 1055–1080.
- Breidt, F. J., R. A. Davis, K.-S. Lh, and M. Rosenblatt (1991). Maximum likelihood estimation for noncausal autoregressive processes. *Journal of Multivariate Analysis* 36(2), 175–198.
- Cavaliere, G., H. B. Nielsen, and A. Rahbek (2020). Bootstrapping noncausal autoregressions: with applications to explosive bubble modeling. *Journal of Business & Economic Statistics* 38(1), 55–67.
- Chan, K.-S., L.-H. Ho, and H. Tong (2006). A note on time-reversibility of multivariate linear processes. *Biometrika* 93(1), 221–227.
- Cubadda, G., F. Giancaterini, A. Hecq, and J. Jasiak (2023). Optimization of the generalized covariance estimator in noncausal processes. *arXiv preprint arXiv:2306.14653*.
- Cubadda, G. and A. Hecq (2011). Testing for common autocorrelation in data-rich environments. *Journal of Forecasting* 30(3), 325–335.
- Davis, R. A. and L. Song (2020). Noncausal vector ar processes with application to economic time series. *Journal of Econometrics* 216(1), 246–267.
- Fries, S. (2022). Conditional moments of noncausal alpha-stable processes and the prediction of bubble crash odds. *Journal of Business & Economic Statistics* 40(4), 1596–1616.
- Fries, S. and J.-M. Zakoian (2019). Mixed causal-noncausal ar processes and the modelling of explosive bubbles. *Econometric Theory* 35(6), 1234–1270.
- Giancaterini, F., A. Hecq, J. Jasiak, and A. M. Neyazi (2025). Regularized generalized covariance (rgcov) estimator. *arXiv preprint arXiv:2504.18678*.
- Giancaterini, F., A. Hecq, and C. Morana (2022). Is climate change time-reversible? *Econometrics* 10(4), 36.
- Giorgis, V., T. A. Huber, and D. Sornette (2024). ‘salvation and profit’: deconstructing the clean-tech bubble. *Technology Analysis & Strategic Management* 36(4), 827–839.

- Gourieroux, C. and J. Jasiak (2016). Filtering, prediction and simulation methods for non-causal processes. *Journal of Time Series Analysis* 37(3), 405–430.
- Gourieroux, C. and J. Jasiak (2017). Noncausal vector autoregressive process: Representation, identification and semi-parametric estimation. *Journal of Econometrics* 200(1), 118–134.
- Gourieroux, C. and J. Jasiak (2023). Generalized covariance estimator. *Journal of Business & Economic Statistics* 41(4), 1315–1327.
- Gourieroux, C. and A. Monfort (2015). Pricing with finite dimensional dependence. *Journal of Econometrics* 187(2), 408–417.
- Gourieroux, C. and J.-M. Zakoian (2017). Local explosion modelling by non-causal process. *Journal of the Royal Statistical Society Series B: Statistical Methodology* 79(3), 737–756.
- Hall, M. and J. Jasiak (2024). Modelling common bubbles in cryptocurrency prices. *working paper at www.jjstats.com*.
- Hecq, A., L. Lieb, and S. Telg (2016). Identification of mixed causal-noncausal models in finite samples. *Annals of Economics and Statistics/Annales d'Économie et de Statistique* (123/124), 307–331.
- Hecq, A. and E. Voisin (2021). Forecasting bubbles with mixed causal-noncausal autoregressive models. *Econometrics and Statistics* 20, 29–45.
- Hecq, A. and E. Voisin (2023). Predicting crashes in oil prices during the covid-19 pandemic with mixed causal-noncausal models. In *Essays in honor of Joon Y. Park: Econometric methodology in empirical applications*, Volume 45, pp. 209–233. Emerald Publishing Limited.
- Hencic, A. and C. Gouriéroux (2015). Noncausal autoregressive model in application to bitcoin/usd exchange rates. *Econometrics of risk*, 17–40.
- Henriques, I. and P. Sadorsky (2008). Oil prices and the stock prices of alternative energy companies. *Energy Economics* 30(3), 998–1010.
- Hull, J. C. and S. Basu (2016). *Options, futures, and other derivatives*. Pearson Education India.

- Jasiak, J. and A. M. Neyazi (2023). Gcov-based portmanteau test. *arXiv preprint arXiv:2312.05373*.
- Khalifa, A. A., A.-J. Ibrahim, A. I. Amhamed, and M. H. El-Naas (2022). Accelerating the transition to a circular economy for net-zero emissions by 2050: a systematic review. *Sustainability* 14(18), 11656.
- Kulik, R. and P. Soulier (2020). *Heavy-tailed time series*. Springer.
- Lanne, M. and P. Saikkonen (2011). Noncausal autoregressions for economic time series. *Journal of Time Series Econometrics* 3(3).
- Lanne, M. and P. Saikkonen (2013). Noncausal vector autoregression. *Econometric Theory* 29(3), 447–481.
- Lof, M. and H. Nyberg (2017). Noncausality and the commodity currency hypothesis. *Energy Economics* 65, 424–433.
- Mohammed, K. S., M. Usman, P. Ahmad, and U. Bulgamaa (2023). Do all renewable energy stocks react to the war in ukraine? russo-ukrainian conflict perspective. *Environmental Science and Pollution Research* 30(13), 36782–36793.
- Phillips, P. C., S. Shi, and J. Yu (2015). Testing for multiple bubbles: Historical episodes of exuberance and collapse in the s&p 500. *International economic review* 56(4), 1043–1078.
- Phillips, P. C., Y. Wu, and J. Yu (2011). Explosive behavior in the 1990s nasdaq: When did exuberance escalate asset values? *International economic review* 52(1), 201–226.
- Sadorsky, P. (2012). Correlations and volatility spillovers between oil prices and the stock prices of clean energy and technology companies. *Energy economics* 34(1), 248–255.
- Wimmer (2016). The green bubble: Our future energy needs and why alternative energy is not the answer.